frontiers | Frontiers in Earth Science

TYPE Original Research
PUBLISHED 23 January 2023
DOI 10.3389/feart.2022.1018675

OPEN ACCESS

EDITED BY
Lucja A. Fostowicz-Frelik,
Institute of Paleobiology (PAN), Poland

REVIEWED BY
Olivier Maridet,
JURASSICA Museum, Switzerland
Lawrence John Flynn,
Harvard University, United States

*CORRESPONDENCE
Xijun Ni,
nixijun@ivpp.ac.cn
Qiang Li,
liqiang@ivpp.ac.cn

SPECIALTY SECTION
This article was submitted to Paleontology, a section of the journal Frontiers in Earth Science

RECEIVED 13 August 2022
ACCEPTED 25 November 2022
PUBLISHED 23 January 2023

CITATION
Ni X, Li Q, Deng T, Zhang L, Gong H, Qin C, Shi J, Shi F and Fu S (2023), New *Yuomys* rodents from southeastern Qinghai-Tibet Plateau indicate low elevation during the Middle Eocene. *Front. Earth Sci.* 10:1018675. doi: 10.3389/feart.2022.1018675

New *Yuomys* rodents from southeastern Qinghai-Tibet Plateau indicate low elevation during the Middle Eocene

Xijun Ni[1,2,3]*, Qiang Li[1,2,3]*, Tao Deng[1,2,3], Limin Zhang[1,2,3], Hao Gong[1,2], Chao Qin[1,2], Jingsong Shi[1], Fuqiao Shi[1] and Shubing Fu[1]

[1]Key Laboratory of Vertebrate Evolution and Human Origins, Institute of Vertebrate Paleontology and Paleoanthropology, Chinese Academy of Sciences, Beijing, China, [2]University of Chinese Academy of Sciences, Beijing, China, [3]CAS Center for Excellence in Life and Paleoenvironment, Beijing, China

Yuomys are medium-sized Hystricomorpha rodents. They are known for coming from areas of low elevation in China during the middle and late Eocene. Two new *Yuomys* were discovered from a locality near Xueshuo village in Litang County, Sichuan Province. The locality lies in the Gemusi pull-apart basin formed in the Litang Fault System (LTFS) in the Hengduan Mountains. The current average elevation is about 4200 m. One of the two new *Yuomys* is larger and shows clear lophodont and unilateral hypsodont morphology, similar to *Yuomys yunnanensis*, which was discovered as being from the early middle Eocene (Irdinmanhan, Asian Land Mammal Ages) in the Chake Basin of Jianshui County, Yunnan Province. The Chake Basin is one of the small pull-apart basins formed in the Xianshuihe-Xiaojiang Fault system (XSH-XJF). The other new *Yuomys* rodent is smaller, brachydont, and less lophodont than the larger new species. The small new *Yuomys* is smaller than all known *Yuomys* except *Yuomys huheboerhensis*, which is from the early middle Eocene Irdinmanhan of Inner Mongolia in Northern China. Given their narrow biochronological distribution and presumably preferred living environment, the occurrence of *Yuomys* in the pull-apart basins in LTFS and XSH-XJF suggests that the two deep fault systems probably started strike-slip movement by the early middle Eocene, about 49–45 million years ago. Well-studied middle Eocene mammalian faunas from Henan and Inner Mongolia include *Yuomys*, primates, and other low elevation forest mammals. We suggest that the two new *Yuomys* species reported here probably also lived in a similar low elevation forest environment.

KEYWORDS

***Yuomys*, Chuandian terrane, accommodation zone, strike-slip movement, plateau uplifting**

1 Introduction

Yuomys is a genus of rodents that existed in the middle and late Eocene in East Asia (Figure 1). Known species of *Yuomys* show a clear evolutionary tendency of developing lophodont and hypodont teeth and increasing body size. The evolutionary sequence of *Yuomys* clearly correlates with the biochronology sequence of Asia (Gong et al., 2021). Apart from the earliest species, *Yuomys huheboerhensis*, later *Yuomys* species are significantly large compared to contemporary rodents, such as ctenodactylids and myomorph rodents. *Y. huheboerhensis* is the oldest-known and the most primitive *Yuomys*. It was discovered from the early middle Eocene Irdin Manha Formation at the Huheboerhe locality in the Huheboerhe-Nuhetingboerhe area of the Erlian Basin of Inner Mongolia (Li and Meng, 2015). *Y. huheboerhensis* is only slightly larger than contemporary ctenodactylids and shows a tendency of developing lophodont teeth. *Yuomys yunnanensis* was discovered from the middle Eocene at the Chake locality near Jianshui County of Yunnan Province. Mammalian fauna correlation suggests that the Chake locality is also Irdinmanhan in age (Huang and Zhang, 1990), probably slightly younger than the fossil site of *Y. huheboerhensis*. *Yuomys weijingensis* was discovered in the Ulan Shireh area of Inner Mongolia. The locality was originally reported as late Eocene, but recent revision of the stratigraphic and mammalian fauna correlations suggest that *Y. weijingensis* should be middle Eocene Irdinmanhan in age (Li and Meng, 2015; Li, 2019; Gong et al., 2021). *Yuomys minggangensis* was discovered from the middle Eocene at the Tuanshan locality near the Xinji Village of Minggang Town, Xinyang City of Henan Province (Wang and Zhou, 1982). The age of the Tuanshan locality is probably also Irdinmanhan. The type species of *Yuomys*, *Yuomys cavioides*, came from the late middle Eocene Sharamurunian at the Rencun locality of Mianchi County, Henan Province (Li, 1975). *Yuomys cf. Y. cavioides* was present at the Ula Usu locality of Inner Mongolia (Li, 1975; Gong et al., 2021), which is Sharamurunian in age. *Yuomys* records of similar age are *Y. eleganes*, *Y. huangzhuangensis*, *Y. altunensis*, and *Y. magnus* from a locality near Dalishu village of Wucheng Town, Tongbai County of Henan Province (Wang, 1978), the Langtougou locality near Huangzhuang village of Qufu City of Shandong Province (Shi, 1989), the Altyn Tagh of Xinjiang Province (Wang, 2017), and the Erden Obo locality of Nomogeng, Siziwangqi County of Inner Mongolia (Li, 2019). The youngest known *Yuomys*, *Y. robustus*, was discovered from the late Eocene at a locality near the Bujiamiaozi village, Lingwu City of Ningxia Province. A specimen from the Zhanglizi Gou locality near Chengliu village of Jiyuan County, Henan Province was recently referred to *Y. robustus* (Gong et al., 2021).

Here we report two new species of *Yuomys* discovered from southeast Qinghai-Tibetan Plateau, where Paleogene mammalian fossils are very rare. Although the two new *Yuomys* species are represented by three specimens only, their morphology clearly distinguishes them from other *Yuomys* and fits in the evolutionary sequence of *Yuomys*. The discovery therefore provides solid evidence for biochronology correlation and paleoenvironmental reconstruction of Southeastern Qinghai-Tibet Plateau.

FIGURE 1
Locality of the Gemusi pull-apart basin and the distribution of *Yuomys*.

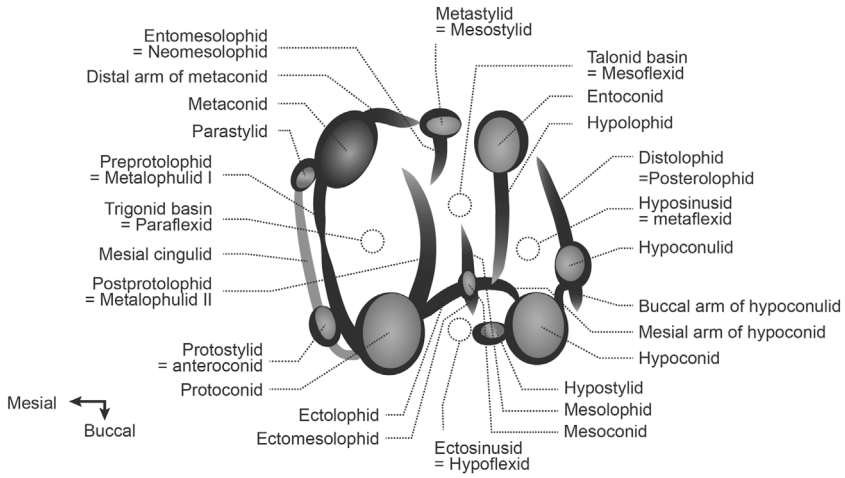

FIGURE 2
Dental terminology used for description and comparison.

2 Materials and methods

The *Yuomys* fossils reported here were discovered from the middle Eocene Gemusi Formation near Xueshuo Village of Litang County, Sichuan Province (Figure 1). The Gemusi Formation sedimentation was developed in the Gemusi pull-apart basin in the Litang Fault System (LTFS). The Gemusi Basin is about 150 km south of Litang city, near the headstream of the Shuiluo river, which is a branch of the Jinsha river. The average elevation of the Gemusi Basin is about 4200 m.

The Gemusi Formation is a set of brownish red-purplish fluvial and lacustrine sediments unconformably overlaying the black Triassic slates (Zong et al., 1996). The remaining thickness of the Gemusi Formation is over 300 m. The lower third of the Gemusi Formation includes conglomerates and coarse sandstones, imbedded with thin layers of mudstones. The middle and upper parts of the Gemusi Formation are dominated by mudstones and sandstone, imbedded with conglomerate layers. There is a thin layer of freshwater limestone in the middle part. There are two mammalian fossil layers. The lower fossil layer only includes some fossil fragments. The upper mammalian fossil layer is within a bed of siltstone enriched with calcareous nodules. The mammalian fossils from this layer include *Anthracokeryx litangensis Bothriodon* sp., *Sianodon* sp., *Caenolophus proficiens*, Brontotheriidae gen. & sp. indet., and the new *Yuomys* species reported here.

The dental morphology terminology used for description and comparison (Figure 2) was modified from Marivaux et al. (2019). Maps were generated at the Conservation Biology Institute Data Basin online mapping system (https://databasin.org/datasets/366a1bef53344c02bcd7d7611d5f61f7/).

3 Systematic paleontology

Class Mammalia Linnaeus, (1758). Order Rodentia Bowdich, (1821). Suborder Hystricomorpha Brandt. (1855). Infraorder Hystricognathi Tullberg, 1899. Family Yuomyidae Dawson et al. (1984). Genus Yuomys Li, 1975. *Yuomys dawai* nov. sp. Ni and Li. LSID urn:lsid:zoobank.org:act:7E3D50A6-A92E-4205-B7C2-A8AF0513A8F9. (Figure 3, Table 1).

Holotype—Specimen IVPP V 31,415, a left lower jaw fragment preserving dp4, m1, and m2.

Type locality—Locality GMS20201010LQ02 (29° 21′ 28.628″N, 100° 28′ 9.665″E), near Xueshuo village, Gemusi Basin, Litang County, Sichuan Province (Figure 1).

Referred specimen—The holotype only.

Age—Early middle Eocene, early Irdinmanhan of Asian Land Mammal Ages, about 49–45 Ma.

Etymology—The species name is dedicated to Dr. Jian'an Dawa, who is a doctor in the Community Hospital at the Xueshuo Village. Dr. Jian'an helped us in the field.

Diagnosis—Small *Yuomys*, brachydont, weakly lophodont. Dp4 mesial cingulid strong, preprotolophid, and postprotolophid enclosing trigonid basin; Dp4-m2 ectolophid oblique, joining the protoconid near buccal side, talonid basin and hyposinusid broad, mesoconid present, mesial arm of hypoconid long; dp4-m1 hypoconulid larger and more projecting than hypoconid; m1 mesolophid present.

Description—Only the holotype is available for description. The jaw preserves a part of the incisor, dp4, m1, and m2. The mental foramen is small and located at a point mesial to the dp4. The inferior masseter ridge is strong. It starts from the lateral side of the m1 and extends inferiorly and posteriorly, and entirely lateral to the incisor alveolar. The inferior masseter ridge extends

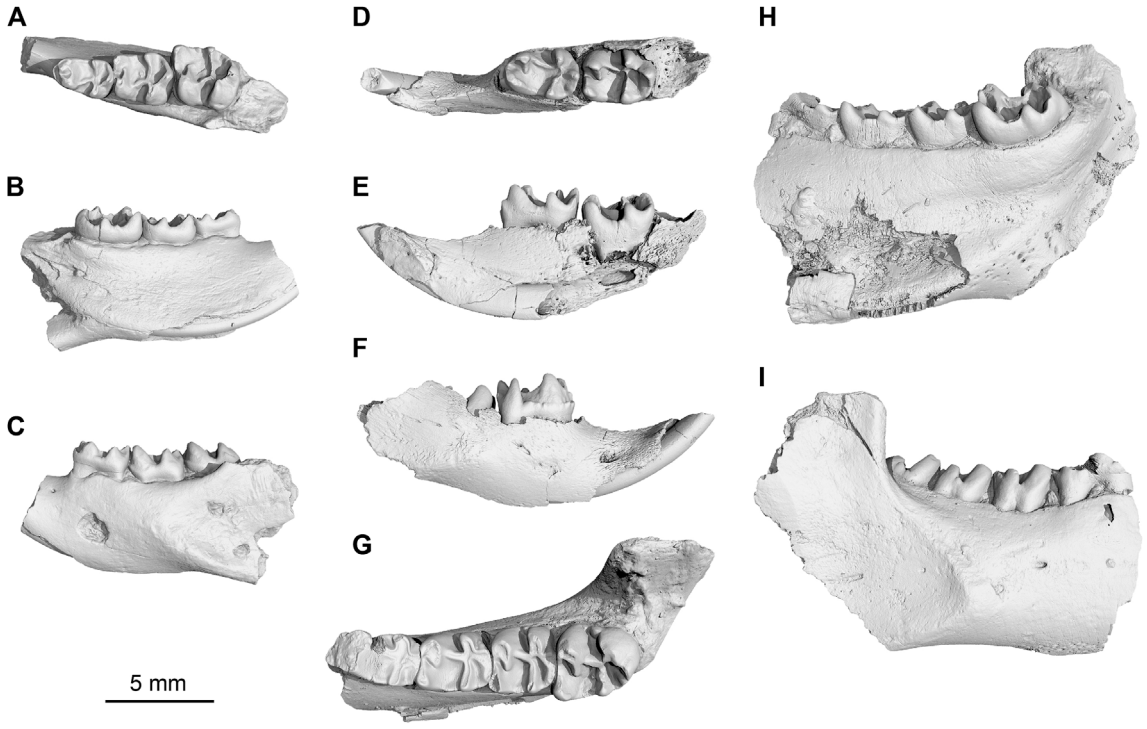

FIGURE 3
New *Yuomys* from the Gemusi pull-apart basin. **(A–C)**, *Yuomys dawai* sp. nov., IVPP V 31415, holotype, in occlusal, lingual, and buccal views; **(D–F)**, *Yuomys gemuensis* sp. nov., IVPP V 31417, in occlusal, lingual, and buccal views; **(G–I)**, *Y. gemuensis* sp. nov., IVPP V 31416, holotype, in occlusal, lingual, and buccal views.

TABLE 1 Measurements of *Yuomys* jaws discovered from the Gemusi Basin (in mm).

	IVPP V 31415			IVPP V 31416			IVPP V 31417		
	Length	Trigonid width	Talonid width	Length	Trigonid width	Talonid width	Length	Trigonid width	Talonid width
dp4	2.86	1.49	1.85	4.35	2.26	2.65	3.74	2.13	2.66
m1	2.99	2.19	2.50	3.46	3.36	3.61	3.43	3.21	3.43
m2	3.10	2.88	3.02	3.27	3.78	3.76			
m3				4.38	4.01	3.50			

to the angular process. Origin of the angular process distinctly buccal to the plane of the incisor alveolus is traditionally defined as hystricognathous jaw (Tullberg, 1899). The ventral side of the incisor has a weak longitudinal enamel stripe.

The buccal side of the check teeth is higher than the lingual size. The overall crown height is low. The dp4 is smaller than the m1 and m2. Its trigonid includes two main cusps, protoconid and metaconid. The two cusps are equal in size, but the metaconid is more mesially positioned. The preprotolophid is short. The buccal and lingual parts of the preprotolophid form a V-shaped notch. The postprotolophid connects the metaconid. The preprotolophid and postprotolophid enclose the trigonid basin. Mesial to the protoconid and metaconid, the mesial cingulid is strong. The dp4 talonid is wider than the trigonid. The talonid basin is broad. The hypoconid is mesial-distally compressed. The entoconid is smoothly fused with the hypolophid. The ectolophid is thin and oblique. It connects the protoconid near the buccal side. A small mesoconid is present in the middle of the ectolophid. The hypolophid connects the ectolophid at a position mesial to the hypoconid.

A short mesial arm of the hypoconid is present. The hypoconulid is larger than the hypoconid and strongly posterior projecting. The hyposinusid is large and deep. A fovea is present buccal and distal to the hypoconid-hypoconulid junction.

The m1 is similar to the dp4, but without mesial cingulid. The preprotolophid is high. The postprotolophid is short. It reaches the metaconid but does not close the trigonid basin completely. The talonid basin is even broader. A weak mesolophid is present. The hypoconulid is even more distally projecting than in the dp4. The hyposinusid almost as broad as the talonid basin.

The m2 is much larger than the m1. Its metaconid is higher and more mesially positioned than the protoconid. The preprotolophid is fused with the metaconid and is relatively higher and stronger than in the m1. The postprotolophid of the m2 is short and does not connect the metaconid. As a result, the distal side of the trigonid is open to the talonid. The talonid is slightly wider than the trigonid. The talonid basin is broad and shallow. The ectolophid is thin and oblique, meeting the protoconid near the buccal margin, as in the dp4 and m1. The mesoconid is weak but visible. There is no mesolophid in the talonid basin. The hypoconid is more mesial-distally compressed than in the dp4 and m1. The mesial arm of the hypoconid is long. The entoconid and hypolophid are fused into a curved ridge. The middle part of the hypolophid is swollen, forming a small cusp. The hypoconulid is smaller and lower than the hypoconid. The hyposinusid is as broad as that of the m1.

Comparison—*Yuomys huheboerhensis* is smaller than all other *Yuomys*. It is characterized by round and low cusps and a relatively square occlusal surface of lower molars. Different from *Y. dawai*, protoconid in *Y. huheboerhensis* has a stronger and higher but relatively shorter buccal part of the preprotolophid and a relatively shorter and weaker postprotolophid. This ridge runs towards the metaconid but does not join the latter cusp. The metaconid of *Y. huheboerhensis* is more mesial-distally compressed. Its buccal part is transformed into the lingual part of the preprotolophid. The buccal and lingual parts of preprotolophid are separated by a shallow notch. In *Y. huheboerhensis*, the lingual preprotolophid is much longer than the buccal preprotolophid. In *Y. dawai*, the metaconid is more conical, and the two parts of the preprotolophid are equally developed. The postprotolophid in *Y. dawai* runs more transversely and joins the base of the metaconid. *Y. huheboerhensis* lacks the mesial cingulid. The hypoconid in *Y. huheboerhensis* is more distal-lingually expanding. In the m1 of *Y. huheboerhensis*, the distal-lingual part of hypoconid is almost fused with the hypoconulid, which is more buccally positioned. There is a sulcus separating the distal-buccal parts of hypoconulid and hypoconid. In *Y. dawai*, the hypoconid is more conical and widely separated from the similarly conical hypoconulid. A longer ridge than that in *Y. huheboerhensis* connects the tips of hypoconid and hypoconulid. The hypoconulid in *Y. dawai* projects distally and is positioned near the middle line. The ectolophid in *Y. huheboerhensis* is short and straight, while it is long and oblique in *Y. dawai*. The mesoconid in *Y. huheboerhensis* is very weak, present as a small swelling on the ectolophid. In *Y. dawai*, the mesoconid is large. In both *Y. huheboerhensis* and *Y. dawai*, the entoconid and hypolophid are fused together. In *Y. huheboerhensis*, the hypolophid is low, and has a weaker connection at the mesial arm of the hypoconid. In *Y. dawai*, the hypolophid is higher and stronger, connecting the distal lingual part of the ectolophid. The talonid basin and ectosinusid buccal to the ectolophid are broader in *Y. dawai* than in *Y. huheboerhensis*.

Yuomys yunnanensis includes a jaw preserving the dp4-m2. The specimen is much larger and has higher crown and stronger cristids than *Y. dawai*. The dp4 of *Y. yunnanensis* has a parastylid and a weak protostylid, two small cusps mesial to the metaconid and protoconid, respectively, but lacks the mesial cingulid. The hypoconulid in *Y. yunnanensis* is less projecting and more buccally positioned than in *Y. dawai*. The buccal end of the hypolophid in *Y. yunnanensis* has a distal turn, which makes the lophid joining the distolophid at the junction between hypoconid and hypoconulid. As a result, the hyposinusid enclosed by the hypolophid and distolophid is much narrower than in *Y. dawai*. In *Y. dawai*, the hypolophid joins the ectolophid at a place mesial to the hypoconid. The m1-2 of *Y. yunnanensis* have squarer occlusal surfaces compared with those of *Y. dawai*. In *Y. yunnanensis*, the preprotolophid is proportionally much higher than that in *Y. dawai*. The m1 postprotolophid in *Y. yunnanensis* runs more distally, therefore the distal side of the trigonid is open. In *Y. dawai*, the m1 postprotolophid extends to the metaconid and closes the trigonid. The ectolophid in *Y. yunnanensis* extends to the tip of metaconid, completely separating the talonid basin and the ectosinusid. The mesolophid and mesoconid are absent. In *Y. dawai*, the ectolophid joins the middle part of the metaconid. The hypolophid in *Y. yunnanensis* joins the ectolophid near the hypoconid, while in *Y. dawai*, the junction is more mesially positioned. In *Y. yunnanensis*, the hyposinusid between the hypolophid and distolophid is narrower than in *Y. dawai*. The hypoconulid in *Y. dawai* is more projecting than in *Y. yunnanensis*.

The Irdinmanhan *Yuomys weijingensis* is probably of similar age to *Y. yunnanensis*. Unfortunately, the specimens of this species were all lost. Available figures and description of the species show that it is less lophodont and about the size of *Y. cavioides* but with more conical cusps.

Yuomys minggangensis includes a jaw fragment preserving the p4-m1. It is much larger than *Y. dawai*, has a squarer occlusal surface, and shows a strong unilateral hypsodonty. In *Y. minggangensis*, the buccal cusps (protoconid and hypoconid) are much larger than the lingual cusps (metaconid and entoconid). The preprotolophid is higher and forms a stronger ridge than in *Y. dawai*. The postprotolophid in *Y. minggangensis* is short and does not close the trigonid. The ectolophid is straighter and shorter than in *Y. dawai*, resulting

in a deeper and narrower ectosinusid. The talonid basin in *Y. minggangensis* is narrower than in *Y. dawai*. The mesoconid and mesolophid is absent in *Y. minggangensis*. The hypolophid is proportionally weaker and joins the joint point between ectolophid and hypoconid. The hypoconulid is less projecting, and the hyposinusid between the hypolophid and distolophid is narrower than in *Y. dawai*.

Yuomys eleganes is represented by a pair of lower jaws and some postcranial fragments. *Y. eleganes* is larger than *Y. dawai*. The occlusal surface of *Y. elegans* is squarer than in *Y. dawai*. Like in other *Yuomys*, the preprotolophid is higher and postprotolophid is shorter in *Y. eleganes* than in *Y. dawai*. The ectolophid in *Y. eleganes* is straighter and shorter. The mesoconid and mesolophid are absent. The talonid basin is narrower than in *Y. dawai*. Being similar to *Y. dawai*, the hypolophid joins the distal part of the ectolophid in *Y. eleganes*. The hypoconulid in *Y. elegans* is present as a swelling of the distolophid. The cusp is not separated from the hypoconid but present as a lingual extension of the hypoconid arm.

Yuomys cavioides is represented by a pair of almost complete lower jaws and two skull fragments preserving the complete upper dentation. *Y. cavioides* is much larger and has higher crown and stronger lophid than *Y. dawai*. In the m1-2 of *Y. cavioides*, the metaconid forms a high lophid and is fused with the buccal part of the preprotolophid. In *Y. dawai*, the metaconid is more conical. The buccal and lingual parts of the preprotolophid are weaker and separated by a notch. The postprotolophid in *Y. dawai* joins the metaconid. In *Y. cavioides*, the postprotolophid is present as a distal-lingual spur of the protoconid. The ectolophid is a high ridge connecting the tips of hypoconid and protoconid in *Y. cavioides*. The ectosinusid and talonid basin are all narrow and deep. No mesolophid and mesoconid are present. In *Y. dawai*, the ectolophid is low and does not extend to the tip of the protoconid. The ectosinusid and talonid basin are broad. A weak mesoconid and a weak mesolophid are present. The hypolophid in *Y. cavioides* is much higher and thicker than that in *Y. dawai*. The hyposinusid enclosed by hypolophid and distolophid is broader and deeper in *Y. dawai*.

Yuomys magnus is much larger than *Y. dawai*. The lower m2s of the two species are the available teeth for comparison. Both have a relatively long occlusal surface. *Y. magnus* has higher tooth crown and stronger lophids. Its hypolophid is stronger but does not connect the ectolophid or hypoconid. The hypoconulid of *Y. magnus* is more conical than in *Y. dawai*.

Yuomys robustus and *Yuomys huangzhuangensis* are known from upper teeth only. They are much larger than *Y. dawai* and have higher tooth crown than *Y. dawai* does.

Yuomys gemuensis nov. sp. Ni and Li. *LSID* urn:lsid:zoobank.org:act:8670E4D0-3DA8-4F67-A306-EA93CF785AD1. (Figure 3, Table 1).

Holotype—Specimen IVPP V 31416, a right lower jaw fragment preserving dp4 and m1-3.

Type locality—Locality GMS20201011SJS01 (29° 21′ 22.000″N, 100° 28′ 25.000″E), near Xueshuo village, Gemusi Basin, Litang County, Sichuan Province (Figure 1).

Referred specimen—IVPP V 31417, a right lower jaw fragment preserving incisor, dp4 and partially erupted m1. From Locality GMS20201011LQ02 (29° 20′ 43.955″N, 100° 28′ 35.899″E), near the Xueshuo Village, Gemusi Basin, Litang County, Sichuan Province (Figure 1).

Age—Early middle Eocene, early Irdinmanhan of Asian Land Mammal Ages, about 49–45 Ma.

Etymology—The specific epithet is from Gemusi, the name of a local lama temple, and the name of the Gemusi Basin.

Diagnosis—Brachydont; Dp4 present mesial and buccal cingulid, mesial metastylid large; Dp4-m2 present buccal arm of hypoconulid; hypolophid thin but well-developed, hypoconulid distally projecting and larger than hypoconid, distal buccal sulcus between hypoconid and hypoconulid deep; m1-3 ectolophid straight, attaching to protoconid distal wall, ectosinusid deep and narrow, hyposinusid broad.

Description—The holotype is a right lower jaw fragment. The preserved inferior masseter ridge root is strong and positioned buccal to the plane of the incisor. The ascending ramus of mandible is vertical and shields the posterior part of the m3. The specimen referred to is a jaw fragment preserving incisor, dp4, and m1. The diastema is thin and long. The mental foramen is mesial to the dp4 and near the incisor. The incisor is gently curved. The enamel is thin. There is a weak longitudinal enamel strip along the ventral side of the incisor. The dp4 is fully erupted but has no wear facet. The m1 is fully developed but still in eruption.

The cheek teeth are brachydont, and weakly lophodont. The buccal side of the cheek teeth is higher than the lingual side. The dp4 has an oval occlusal shape. Its trigonid is narrower than the talonid. The metaconid is buccal-lingually compressed. The tip of metaconid is higher and more mesially positioned than the protoconid. The distal arm of the metaconid is strong. The buccal and lingual parts of the preprotolophid is separated by a deep V-shaped notch. The postprotolophid is short and does not connect the metaconid, therefore the distal wall of the trigonid (postvallid) is open. The mesial cingulid is strong. It extends from the mesial side of the metaconid to the protoconid and becomes a weak buccal cingulid and ends at the mesial side of the hypoconid. A small parastylid is present at the lingual end of the mesial cingulid. There is also an incipient protostylid mesial to the protoconid. The talonid has a broad basin. Its lingual border has a low rim. The hypoconid is conical. Its mesial arm is very short. The entoconid is also conical, but its buccal side is fused into the hypolophid. The hypolophid buccally joins the distal arm of the hypoconid, instead of ectolophid. The ectolophid is thin and oblique. Its mesial part ends in the distobuccal side of the protoconid but does not extends to the

tip of the protoconid. The ectosinusid is deep and narrow. The hypoconulid is large and higher than the hypoconid. A strong and blunt buccal arm of hypoconulid is present. There is a deep and broad sulcus enclosed by the hypoconid, hypoconulid, and the buccal arm of the hypoconulid. The hyposinusid is broad.

The m1 has a rectangular occlusal shape. The trigonid and talonid are similar in width. The protoconid is robust and conical. The metaconid is mesial-distally compressed and fused with the preprotolophid. The postprotolophid is short and does not connect the metaconid. The talonid basin is broad. The hypoconid is mesial-distally compressed. Its mesial arm is very short. The entoconid is also mesial-distally compressed. It is fully fused with the hypolophid. The entoconid, hypolophid, and hypoconid form a transverse ridge. The ectolophid is straight. It connects the distal wall of the protoconid but does not extend to the protoconid tip. The ectosinusid between the protoconid and hypoconid is deep and narrow. The hypoconulid is much larger than the hypoconid. The buccal arm of the hypoconulid is strong. The sulcus buccal-distal to the joint of hypoconid and hypoconulid is relatively shallower and narrower than that of dp4. The m2 is smaller than the m1 and has a squarer occlusal shape than the m1. The cusp shape and ridge arrangement are similar to those of the m1. Because the tooth is relatively short, the talonid basin, ectosinusid, and hyposinusid of the m2 are all narrower than those of the m1. Between the metaconid and entoconid, the talonid basin border has a thicker rim and develops an incipient metastylid. The ectosinusid has a low buccal rim. There is an incipient hypostylid on the rim. The m3 is much larger than the m1 and m2. The m3 talonid is narrower than the trigonid, and the distal side of the tooth is rounded. Different from the m1 and m2, the protoconid and hypoconid of the m3 are more conical, and the ridges are thicker. The hypoconulid is less projecting and smaller than the hypoconid. There is a cusp-like swelling on the hypolophid. The metastylid and hypostylid are large.

Comparison—*Yuomys gemuensis* is more similar to *Y. yunnanensis* than to other *Yuomys* species. The dp4 of *Y. gemuensis* has a mesial cingulid and a buccal cingulid. The two cingulids are absent in *Y. yunnanensis*. The paratylid in *Y. gemuensis* is relatively smaller than that in *Y. yunnanensis*, and the protostylid is present as a nodule on the mesial cingulid. The hypoconid in *Y. yunnanensis* is more buccally expanded than in *Y. gemuensis*. The hypoconulid is less distally projecting. As a result, the distal valley enclosed by hypoconulid and hypolophid is narrower than in *Y. gemuensis*. A buccal arm rises from the buccal side of the hypoconulid in *Y. gemuensis*. The m1s of *Y. gemuensis* and *Y. yunnanensis* are similar in size and morphology. Slightly different from *Y. gemuensis*, the hypolophid in *Y. yunnanensis* is weaker, and the distal buccal sulcus between the hypoconid and hypoconulid is shallower. The m2 of *Y. yunnanensis* is proportionally larger than the m2 of *Y. gemuensis*. As in the m1, the m2 hypolophid in *Y. yunnanensis* is weaker and the distal buccal sulcus between the hypoconid and hypoconulid is shallower than in *Y. gemuensis*. The ectolophid extends to the tip of protoconid in *Y. yunnanensis*. In *Y. gemuensis*, the ectolophid does not extend to the tip of protoconid.

Yuomys huheboerhensis is much smaller and has more conical cusps than *Y. gemuensis*. The lingual and buccal preprotolophid of molars are separated by a notch in *Y. huheboerhensis*. In *Y. gemuensis*, the lingual and buccal preprotolophid are fused into a strong ridge connecting the protoconid and metaconid. As in *Y. gemuensis*, the ectolophid in *Y. huheboerhensis* does not extend to the tip of protoconid. A rudimentary mesoconid is present in some individuals in *Y. huheboerhensis*, but it is totally absent in *Y. gemuensis*. The talonid basin in *Y. huheboerhensis* is relatively broader than in *Y. gemuensis*. The hypolophid in *Y. huheboerhensis* is very weak. Its buccal end does not join the ectolophid, or has only a weak connection. Similar to *Y. gemuensis*, but different from most other *Yuomys*, the hypoconulid is more buccally positioned, and usually has a deep distal buccal notch separating it from the hypoconid in the m1-2. Different from *Y. gemuensis*, the m1-2 hypoconulid in *Y. huheboerhensis* barely projects above the hypoconid.

Yuomys minggangensis is much bigger than *Y. gemuensis* and shows stronger unilateral hyposodonty. The protoconid, metaconid, and hypoconid of *Y. minggangensis* are more conical and robust than those of *Y. gemuensis*. The entoconid and the hypolophid of *Y. minggangensis* are relatively weaker. The ectolophid in *Y. minggangensis* is short and straight, proportionally stronger than in *Y. gemuensis*. The hypoconulid of the m1 in *Y. minggangensis* is smaller than the hypoconid, whereas in *Y. gemuensis*, the hypoconulid is larger than hypoconid. The distal buccal side of the hypoconulid in *Y. minggangensis* lacks a buccal arm as in *Y. gemuensis*. In *Y. minggangensis*, the hyposinusid enclosed by the distolophid and hypolophid is also proportionally smaller.

Yuomys eleganes is of roughly the same size as *Y. gemuensis*. The cusps and ridges of both taxa are also equally developed. The m1-2 of *Y. eleganes* are deeply worn. Detailed morphology is not available for comparison. However, it is obvious that the hypolophid in *Y. eleganes* is more mesially positioned, and the talonid basin is narrower than in *Y. gemuensis*. The hypoconulid in *Y. eleganes* is probably fused with the hypoconid and present as an extension of the distal arm of hypoconid. No trace of sulcus is present between the hypoconid and hypoconulid. A small hypostylid in the ectosinusid mesial to the hypoconid is present in both taxa. The m3 of *Y. gemuensis* is of slightly bigger size. In both taxa, the preprotolophid is high, and the postprotolophid is a short spur. The m3 hypolophid connects the middle of the ectolophid in *Y. eleganes*, whereas the lophid joins the ectolophid near hypoconid in *Y. gemuensis*. As a result, the m3 talonid basin in *Y. eleganes* is narrower. There is a small metastylid mesial to the entoconids on the lingual edge of the talonid basin in *Y. eleganes*. This small cusp almost closes the lingual side of the

talonid basin. Similarly in *Y. gemuensis*, the lingual side of the talonid basis has a low and blunt rim, and the metastylid is also present. In the ectosinusid and mesial to the hypoconid, there is a small hypostylid in both taxa. The m3 hypoconulid in *Y. eleganes* is present as a swelling of the hypoconid distal lingual arm (distal lophid). There is no sulcus defining the border between hypoconid and hypoconulid, and probably no projection from the arm. In *Y. gemuensis*, the hypoconulid clearly projects above the distal lophid and is separated from the hypoconid by a shallow sulcus distal lingual to the junction between hypoconid and hypoconulid.

Yuomys cavioides is larger, more hypsodont and lophodont than *Y. gemuensis*. The postprotolophid is longer in *Y. cavioides* than in *Y. gemuensis*. The m3 postprotolophid in *Y. cavioides* is particularly longer, which reaches the lingual side of the hypolophid. The m1-3 ectolophids in *Y. cavioides* all extend to the tips of protoconid. The hypolophids are more mesially positioned and proportionally higher than in *Y. gemuensis*. The talonid basin and ectosinusid in *Y. cavioides* are narrower and deeper. The small hypostylid mesial to the hypoconid as that in *Y. gemuensis* is absent in *Y. cavioides*. A small metastylid mesial to the entoconid along the lingual tooth border of the m2-3 is present in *Y. cavioides* but is weaker in *Y. gemuensis*. The hypoconulid of the m1-2 is slightly smaller than hypoconid in *Y. cavioides*, whereas it is bigger than hypoconid in *Y. gemuensis*. The sulcus distal buccal to the junction between hypoconid and hypoconulid of the m1-2 in *Y. gemuensis* is deeper than that in *Y. cavioides*. The buccal ridge-like arm from hypoconulid is present in the m1-2 of *Y. gemuensis* but absent in *Y. cavioides*. The lingual extension of the distolophid is longer in *Y. gemuensis* than in *Y. cavioides*. The m3 hypoconulids and distolophids are equally developed in both taxa. Both have a shallow sulcus distal buccal to the junction between hypoconid and hypoconulid. This sulcus is absent in other *Yuomys*.

Yuomys magnus is larger than *Y. gemuensis*. The tooth crown of *Y. magnus* is higher than *Y. gemuensis*. The m2-3 ectolophid of *Y. magnus* is oblique and connects the protoconid near the buccal side. As a result, the m2-3 ectosinusid of *Y. magnus* is shallower and oblique. The m2 hypolophid of *Y. magnus* does not connect the ectolophid or hypoconid. The m3 hypolophid of *Y. magnus* has a weaker connection to the ectolophid than in *Y. gemuensis*. In *Y. gemuensis*, the m2 hypoconulid has a buccal arm that forms a transverse ridge from hypoconulid. The sulcus between this buccal arm and hypoconid is deep. In *Y. magnus*, the m2 hypoconid is conical and lacks a buccal extension.

Yuomys robustus is known from upper teeth only. It is much larger than *Y. gemuensis* and has higher tooth crown. *Yuomys huangzhuangensis* is also known from the upper teeth only. Its size matches that of *Y. gemuensis*. Relatively thicker ridges of *Y. huangzhuangensis* upper teeth suggest that the lower teeth of this species should also have thicker ridges than *Y. gemuensis*.

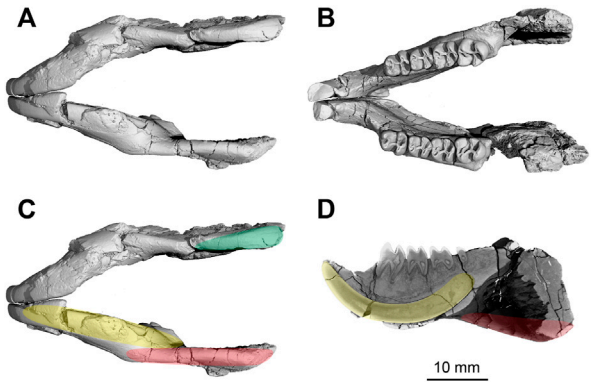

FIGURE 4
The low jaw of the type specimen of *Yuomys cavioides* (IVPP V 4796.1-2), showing the hystricognathous form. **(A)**, ventral view; **(B)**, occlusal view: **(C)**, yellow shadow indicating the plane of the incisive alveolus, red shadow indicating the plane of the angular process being distinctly lateral to the plane of the incisive alveolus, green shadow indicating expanded ventral edge of the angular process; **(D)**, virtual section of the right half mandible in medial view, yellow shadow indicting the posterior extension of the incisor, red shadow indicating the angular process.

4 Discussion

Huchon et al. (2000) defined "Ctenohystrica" as a suborder of Rodentia based on molecular evidence. Initially Ctenohystrica was defined as a crown-group that includes the least-inclusive clade of all extant family Ctenodactylidae and infraorder Hystricognathi. Marivaux et al. (2004) and Flynn et al. (2019) redefined Ctenohystrica as a more inclusive group that includes stem and extant Hystricognathi, stem and extant sciurognathous Ctenodactylidae, and all extant or extinct groups more closely related to them than to other sciurognathous rodents. Blanga-Kanfi et al. (2009) revised the rodent phylogeny based on the combined nucleotide datasets and supported the monophyly of Ctenohystrica. It is not difficult to see that the main connotation of Ctenohystrica has no difference with the traditional Hystricomorpha. Here we follow the systematic of Wilson and Reeder (2005) by using suborder Hystricomorpha. *Yuomys* are moderately diverse Eocene rodents. The taxonomy and distribution of *Yuomys* have been revised recently (Gong et al., 2021). Previously, *Yuomys* was considered as a rodent with a hystricomorphous skull but with a hystricognathous jaw. For this reason, *Yuomys* was traditionally assigned in the "trash bin" high level taxon Ctenodactyloidea. Our re-observation on the lower jaw of the type specimen of *Yuomys cavioides* revealed that this specimen is actually hystricognathous (Figure 4). In living hystricognaths, the origin of the angular process is distinctly lateral to the plane of the incisor alveolus. The inferior margin of the angular process is generally wide, and the reflexa part of lateral masseter passes around the ventral

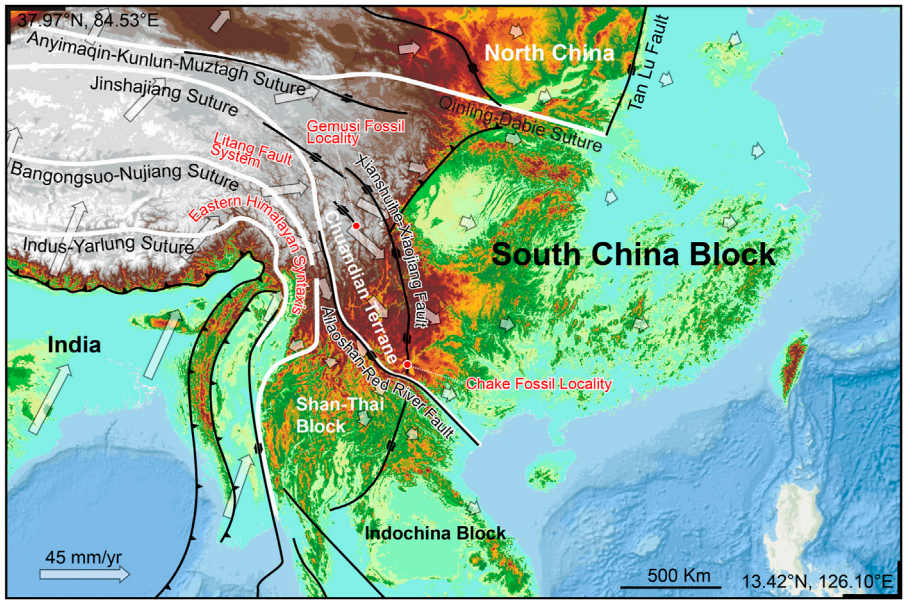

FIGURE 5
Chuandian Terrane and the major faults in the accommodation zone in the southeastern margin of Qinghai-Tibet Plateau. Hollow arrows indicating modern GPS velocity field (based on Wang and Shen 2020).

surface of the angular process to insert on the medial side of the angular process (Tullberg, 1899; Wood, 1985). The angular process of the type specimen of *Y. cavioides* is well preserved. The plane of angular process is clearly lateral to the plane of the incisive alveolus (Figure 4). The ventral edge of the angular process is widened (Figure 4) in a form generally present in living hystricognaths. We therefore categorized *Yuomys* and Yuomyidae as the infraorder Hystricognathi.

Yuomys dawai is much smaller with a lower tooth crown than other *Yuomys* species except *Yuomys huheboerhensis*. Compared to *Y. huheboerhensis*, *Y. dawai* shows more typical *Yuomys* features, suggesting that the sediments bearing *Y. dawai* is probably younger than that of *Y. huheboerhensis*, but it is still older than other *Yuomys*. *Yuomys gemuensis* and *Yuomys yunnanensis* from the Chake pull-apart basin closely resemble each other and both show similar development of tooth crown height and ridges. The similar evolutionary grade shared by these two species suggests that the fossil layers bearing the two *Yuomys* have the same mammalian age: early Irdinmanhan of Asian Land Mammal Age (about 49–45 Ma).

It has been demonstrated that about 1300–2500 km of the northward convergence between the Indian plate with the continent of Eurasia caused widespread crustal deformation, including mountain building, plate shortening, and plateau uplifting (Molnar and Stock, 2009; Copley et al., 2010; Cande and Stegman, 2011; van Hinsbergen et al., 2011; Tong et al., 2015; Yao et al., 2015; Ding et al., 2017; Wang and Shen, 2020). The most intriguing feature of this widespread crustal deformation is reflected by clockwise rotation of southeastern Qinghai-Tibet Plateau around the Eastern Himalayan Syntaxis (EHS) and lateral escape of crustal materials on the southeastern edge of the plateau relative to the rigid South China Block (Yin and Harrison, 2000; Tapponnier et al., 2001; Molnar and Stock, 2009; Copley et al., 2010; Cande and Stegman, 2011; van Hinsbergen et al., 2011; Tong et al., 2015). One theory is that the outward expansion along major strike-slip faults (such as Xianshuihe-Xiaojiang Fault, Litang Fault System, Three Rivers Faults, and Red River Fault) and clockwise strike-slip processes around EHS occur at the mantle scale (Tapponnier et al., 2001; Zhang et al., 2021). The development of the Cenozoic extensional intermountain basins in the southeast margin of Qinghai-Tibetan Plateau is kinematically linked with the strike-slip faults, and the sedimentation in these basins can provide important age constraints for the timing of fault development and orogenic processes (Li et al., 2015; Li et al., 2020).

The southeastern margin of Qinghai-Tibet Plateau was one of the most important accommodation zones during the India-Eurasia collision. The temporal and spatial evolution of the zone is tightly correlated with the crustal deformation and high topography evolution of Qinghai-Tibet Plateau (Figure 5). This accommodation zone comprises the Shan Thai Block (STB), Indochina Block (ICB), and Chuandian Terrane (CDT), which consists of fragments from the western part of South China Block (SCB) and the southern part of Songpan Ganzi fold belt (Wang et al., 1998; Wang et al., 2014; Tong et al., 2015). The CDT is separated from the relatively stable SCB in the north and northeast by the Xianshuihe-Xiaojiang Fault (XSH-XJF), and from the STB and ICB in the south and southwest by

the Ailao Shan-Red River Fault (ASRRF) (Wang et al., 1998; Tong et al., 2015; Li et al., 2017; Li et al., 2020).

The *Yuomys* fossils reported here were discovered from the Gemusi pull-apart basin, which was formed within the northwest striking LTFS. This fault system is located between the XSH-XJF to the north and ASRRF to the south. Its activity is controlled by the two latter faults (Chevalier et al., 2016). The *Yuomys* fossil from the Chake was discovered from a locality in the Chake pull-apart basin, which was formed within the southern end of the XSH-XJF. Similarities shared by the *Yuomys* from Gemusi and Chake suggest that they lived during the same geological epoch and similar adaptive environment, and consequently suggest that the Gemusi Basin and Chake Basin were formed roughly in the same period (about 49–45 Ma).

In a recent study, the mammalian fossil localities in the Gemusi Basin, which were reported in Zong et al. (1996), were wrongly pinned, and the fossil layer of Gemusi Formation was wrongly correlated to the upper part of the Relu Formation of the nearby Relu Basin (He et al., 2022). Our field tracing and previous stratigraphic correlations (Chen et al., 1983; Guo, 1986; Zong et al., 1996) indicate that the mammalian fossil layer of the Gemusi Formation should be correlated with the lower part of the Relu Formation (equivalent to the Changzong Formation in He et al., 2022), below the plant fossil strata of the Relu Formation. U-Pb dating of the zircons from the volcanic tuffs imbedded in the plant fossil layers of the Relu Formation showed an age of 42–40 Ma, and U-Pd dating of the zircons from the sandstone of the lower part of the Relu Formation indicated that the maximum depositional age is about 50 Ma (He et al., 2022). These dating results are consistent with our biochronological estimation.

Present-day CDT is characterized by clockwise rotation around EHS as revealed by GPS velocities (Figure 5, Zhang et al., 2004; Wang and Shen, 2020; Xu et al., 2022). A maximum shear strain rate of 40–60 nanostrain/yr is found along the XSH-XJF (Wang and Shen, 2020). The initiation timing of the strike-slip movement of XSH-XJF and ASRRF and the formation of the CDT is controversial. It was suggested that the CDT remained relatively stable and did not begin rotational extrusion movement before 17 Ma (Tong et al., 2015), while some other research suggested that the crustal deformation of the CDT began at ~ 35 Ma (Li et al., 2020). The *Yuomys* fossils from CDT constrain the timing of sedimentation within the Gemusi pull-apart basin and Chake pull-apart basin. Our paleontological evidence suggests that the initiation of CDT crustal movement could be earlier than 49 Ma.

The occurrence of *Yuomys* in CDT may suggest that the area had a lowland tropical environment during the middle Eocene. It is known that *Yuomys* occurred with small-sized stem anthropoid and tarsiiform primates, in, for example, the Mianchi-Yuanqu Basin in Henan Province and Erlian Basin in Inner Mongolia (Beard, 1998; Beard and Wang, 2004; Ni, 2010; Wang et al., 2018). Living and fossilized small primates are known to occur only in lowland tropical forest or jungle environments (Fleagle, 2013; Li and Ni, 2016; Ni et al., 2016). Plant fossils from the nearby Relu Formation indicate a lowland tropical environment (Chen et al., 1983; Guo, 1986; Su et al., 2009; He et al., 2022). It is therefore likely that the uplift of CDT and the strike-slip movement of XSH-XJF and ASRRF were not synchronous.

Data availability statement

The original contributions presented in the study are included in the article/supplementary material, further inquiries can be directed to the corresponding authors.

Author contributions

XN analyzed the data and wrote the manuscript. QL analyzed the data and edited the manuscript. TD analyzed the data. LZ, HG, and CQ CT-scanned the fossil. JS, FS, and SF collected data.

Funding

This project was supported by the Second Tibetan Plateau Scientific Expedition and Research Program (2019QZKK705), the National Natural Science Foundation of China (41988101, 41888101, 41625005), the Strategic Priority Research Program of Chinese Academy of Sciences (CAS XDB26030300, XDA20070203, XDA19050100).

Acknowledgments

We thank T. Stidham for comments and English-language editing. We thank Qian Li, Lawrence J. Flynn, and Olivier Maridet for comments and discussion.

Conflict of interest

The authors declare that the research was conducted in the absence of any commercial or financial relationships that could be construed as a potential conflict of interest.

Publisher's note

References

Beard, K. C. (1998). A new genus of tarsiidae (Mammalia: Primates) from the middle Eocene of shanxi Province, China, with notes on the historical biogeography of tarsiers. *Bull. Carnegie Mus. Nat. Hist.* 34, 260–277.

Beard, K. C., and Wang, J. (2004). The eosimiid primates (anthropoidea) of the heti formation, Yuanqu Basin, shanxi and henan provinces, people's republic of China. *J. Hum. Evol.* 46, 401–432. doi:10.1016/j.jhevol.2004.01.002

Blanga-Kanfi, S., Miranda, H., Penn, O., Pupko, T., Debry, R. W., and Huchon, D. (2009). Rodent phylogeny revised: Analysis of six nuclear genes from all major rodent clades. *BMC Evol. Biol.* 9, 71. doi:10.1186/1471-2148-9-71

Bowdich, T. E. (1821). *An analysis of the natural classifications of Mammalia, for the use of students and travellers*. Paris: J. Smith.

Brandt, J. F. (1855). Beiträge zur nähern Kenntniss der Säugethiere Russlands *St. Pétersbourg*. Saint Petersburg,Russia: De l'Imprimerie de l'Académie impériale des sciences.

Cande, S. C., and Stegman, D. R. (2011). Indian and African plate motions driven by the push force of the Réunion plume head. *Nature* 475, 47–52. doi:10.1038/nature10174

Chen, M., Kong, Z., and Chen, Y. (1983). On the discovery of palaeogene flora from the Western Sichuan Plateau and its significance in phytogeography. *Acta Bot. Sin.* 25, 482–491.

Chevalier, M.-L., Leloup, P. H., Replumaz, A., Pan, J., Liu, D., Li, H., et al. (2016). Tectonic-geomorphology of the Litang fault system, SE Tibetan Plateau, and implication for regional seismic hazard. *Tectonophysics* 682, 278–292. doi:10.1016/j.tecto.2016.05.039

Copley, A., Avouac, J.-P., and Royer, J.-Y. (2010). India-Asia collision and the Cenozoic slowdown of the Indian plate: Implications for the forces driving plate motions. *J. Geophys. Res.* 115, B03410. doi:10.1029/2009jb006634

Dawson, M. R., Li, C., and Qi, T. (1984). Eocene ctenodactyloid rodents (Mammalia) of eastern central Asia. *Carnegie Mus. Nat. Hist. Special Publ.* 9, 138–150.

Ding, L., Satybaev, M., Cai, F., Wang, H., Song, P., Ji, W.-Q., et al. (2017). Processes of initial collision and suturing between India and Asia. *Sci. China Earth Sci.* 60, 635–651. doi:10.1007/s11430-016-5244-x

Fleagle, J. G. (2013). *Primate adaptation and evolution*. Third Edition. New York: Academic Press.

Flynn, L. J., Jacobs, L. L., Kimura, Y., and Lindsay, E. H. (2019). Rodent suborders. *Foss. Impr.* 75, 292–298. doi:10.2478/if-2019-0018

Gong, H., Li, Q., and Ni, X. (2021). New species of Yuomys (Rodentia, ctenodactyloidea) from the upper Eocene of eastern Ningxia, China. *J. Vertebrate Paleontology* 41, e1938099. doi:10.1080/02724634.2021.1938099

Guo, S. (1986). "An Eocene flora from the Relu Formation in Litang county of sichuan and the history of Eucalyptus," in *The comprehensive scientific expedition to the qinghai-xizang plateau. Studies in qinghai-xizang (tibet) plateau. Special issue of hengduan mountains scientific expedition (II)*. Editor T. C. A. S. O. (Beijing: Beijing Science & Technology Press).

He, S., Ding, L., Xiong, Z., Spicer, R. A., Farnsworth, A., Valdes, P. J., et al. (2022). A distinctive Eocene Asian monsoon and modern biodiversity resulted from the rise of eastern Tibet. *Sci. Bull.* 67, 2245–2258. doi:10.1016/j.scib.2022.10.006

Huang, X., and Zhang, J. (1990). First record of early tertiary mammals from southern yunnan. *Vertebr. Palasiat.* 28, 296–303.

Huchon, D., Catzeflis, F. M., and Douzery, E. J. P. (2000). Variance of molecular datings, evolution of rodents and the phylogenetic affinities between Ctenodactylidae and Hystricognathi. *Proc. R. Soc. Lond. B* 267, 393–402. doi:10.1098/rspb.2000.1014

Li, C. (1975). *Yuomys*, a new ischyromyoid rodent genus from the upper Eocene of North China. *Vertebr. Palasiat.* 13, 58–70.

Li, Q. (2019). Eocene ctenodactyloid rodent assemblages and diversification from erden Obo, nei mongol, China. *Hist. Biol.* 31, 813–823. doi:10.1080/08912963.2017.1395422

Li, Q., and Meng, J. (2015). New ctenodactyloid rodents from the Erlian Basin, nei mongol, China, and the phylogenetic relationships of Eocene asian ctenodactyloids. *Am. Mus. Novitates* 3828, 1–20. doi:10.1206/3828.1

Li, Q., and Ni, X. (2016). An early Oligocene fossil demonstrates treeshrews are slowly evolving "living fossils". *Sci. Rep.* 5, 18627. doi:10.1038/srep18627

Li, S., Advokaat, E. L., Van Hinsbergen, D. J. J., Koymans, M., Deng, C., and Zhu, R. (2017). Paleomagnetic constraints on the Mesozoic-Cenozoic paleolatitudinal and rotational history of Indochina and South China: Review and updated kinematic reconstruction. *Earth-Science Rev.* 171, 58–77. doi:10.1016/j.earscirev.2017.05.007

Li, S., Deng, C., Dong, W., Sun, L., Liu, S., Qin, H., et al. (2015). Magnetostratigraphy of the Xiaolongtan Formation bearing Lufengpithecus keiyuanensis in Yunnan, southwestern China: Constraint on the initiation time of the southern segment of the Xianshuihe–Xiaojiang fault. *Tectonophysics* 655, 213–226. doi:10.1016/j.tecto.2015.06.002

Li, S., Su, T., Spicer, R. A., Xu, C., Sherlock, S., Halton, A., et al. (2020). Oligocene deformation of the chuandian Terrane in the SE margin of the Tibetan plateau related to the extrusion of Indochina. *Tectonics* 39, e2019TC005974. doi:10.1029/2019tc005974

Linnaeus, C. (1758). *Systema naturæ per regna tria naturæ, secundum classes, ordines, genera, species, cum characteribus, differentiis, synonymis, locis*. Washington, DC, USA: Biodiversity heritage library. Editio Decima, Holmiæ, (Impensis direct. Laurentii Salvii).

Marivaux, L., and Boivin, M. (2019). Emergence of hystricognathous rodents: Palaeogene fossil record, phylogeny, dental evolution and historical biogeography. *Zoological J. Linn. Soc.* 187, 929–964. doi:10.1093/zoolinnean/zlz048

Marivaux, L., Vianey-Liaud, M., and Jaeger, J.-J. (2004). High-level phylogeny of early tertiary rodents: Dental evidence. *Zoological J. Linn. Soc.* 142, 105–134. doi:10.1111/j.1096-3642.2004.00131.x

Molnar, P., and Stock, J. M. (2009). Slowing of India's convergence with Eurasia since 20 Ma and its implications for Tibetan mantle dynamics. *Tectonics* 28. doi:10.1029/2008tc002271

Ni, X., Li, Q., Li, L., and Beard, K. C. (2016). Oligocene primates from China reveal divergence between African and Asian primate evolution. *Science* 352, 673–677. doi:10.1126/science.aaf2107

Ni, X., Meng, J., Beard, K. C., Gebo, D. L., Wang, Y., and Li, C. (2010). A new tarkadectine primate from the Eocene of inner Mongolia, China: Phylogenetic and biogeographic implications. *Proc. R. Soc. B* 277, 247–256. doi:10.1098/rspb.2009.0173

Shi, R. (1989). Late Eocene mammalian fauna of Huangzhuang, Qufu, Shandong. *Vertebr. Palasiat.* 27, 87–102.

Su, T., Xing, Y., Yang, Q., and Zhou, Z. (2009). Reconstruction of mean annual temperature in Chinese Eocene paleofloras based on leaf margin analysis. *Acta Palaeontol. Sin.* 48, 65–72.

Tapponnier, P., Zhiqin, X., Roger, F., Meyer, B., Arnaud, N., Wittlinger, G., et al. (2001). Oblique stepwise rise and growth of the Tibet Plateau. *Science* 294, 1671–1677. doi:10.1126/science.105978

Tong, Y.-B., Yang, Z., Wang, H., Gao, L., An, C.-Z., Zhang, X.-D., et al. (2015). The Cenozoic rotational extrusion of the Chuan Dian Fragment: New paleomagnetic results from Paleogene red-beds on the southeastern edge of the Tibetan Plateau. *Tectonophysics* 658, 46–60. doi:10.1016/j.tecto.2015.07.007

Tullberg, T. (1899). Ueber das system der Nagethiere: Eine phylogenetische studie. *Nova Acta Regiae Soc. Sci. Ups.* 18, 1–514.

Van Hinsbergen, D. J. J., Kapp, P., Dupont-Nivet, G., Lippert, P. C., Decelles, P. G., and Torsvik, T. H. (2011). Restoration of cenozoic deformation in Asia and the size of greater India. *Tectonics* 30. doi:10.1029/2011tc002908

Wang, B. (2017). Discovery of *Yuomys* from altun Shan, Xinjiang, China. *Vertebr. Palasiat.* 55, 227–232.

Wang, B., and Zhou, S. (1982). Late Eocene mammals from pingchangguan basin, henan. *Vertebr. Palasiat.* 20, 203–215.

Wang, E., Burchfiel, B. C., Royden, L. H., Liangzhong, C., Jishen, C., Wenxin, L., et al. (1998). Late cenozoic xianshuihe-xiaojiang, Red River, and dali fault systems of southwestern sichuan and central yunnan, China. *Geol. Soc. Am.* 327. doi:10.1130/SPE327

Wang, E., Meng, K., Su, Z., Meng, Q., Chu, J. J., Chen, Z., et al. (2014). Block rotation: Tectonic response of the Sichuan basin to the southeastward growth of the Tibetan Plateau along the Xianshuihe-Xiaojiang fault. *Tectonics* 33, 686–718. doi:10.1002/2013tc003337

Wang, J. (1978). Fossil amynodontidae and ischyromyidae of tongbo, henan. *Vertebr. Palasiat.* 16, 22–29.

Wang, M., and Shen, Z.-K. (2020). Present-day crustal deformation of continental China derived from GPS and its tectonic implications. *J. Geophys. Res. Solid Earth* 125, e2019JB018774. doi:10.1029/2019jb018774

Wang, Y., Li, Q., Bai, B., Jin, X., Mao, F., and Meng, J. (2018). Paleogene integrative stratigraphy and timescale of China. *Sci. China Earth Sci.* 62, 287–309. doi:10.1007/s11430-018-9305-y

Wilson, D. E., and Reeder, D. M. (2005). "Mammal species of the world, literature cited," in *Mammal species of the world. A taxonomic and geographic reference*. Editor D. E. W. D. M. REEDER 3rd edition (Baltimore, MD, USA: Johns Hopkins University Press).

Wood, A. E. (1985). "The relationships, orgin and dispersal of the hystricognathous rodents," in *Evolutionary relationships among rodents. A multidisciplinary analysis*. Editors W. P. LUCKETT and J.-L. HARTENBERGER (New York: Springer Science+Business Media, LLC).

Xu, B.-B., Wang, Y., Zhang, Z.-Q., Yan, Y.-G., He, X.-H., Hao, M., et al. (2022). Slip distribution and block rotation of the Indo-South China region inferred from GNSS analyses. *J. Asian Earth Sci.* 233, 105206. doi:10.1016/j.jseaes.2022.105206

Yao, T., Wu, F., Ding, L., Sun, J., Zhu, L., Piao, S., et al. (2015). Multispherical interactions and their effects on the Tibetan plateau's Earth system: A review of the recent researches. *Natl. Sci. Rev.* 2, 468–488. doi:10.1093/nsr/nwv070

Yin, A., and Harrison, T. M. (2000). Geologic evolution of the himalayan-Tibetan orogen. *Annu. Rev. Earth Planet. Sci.* 28, 211–280. doi:10.1146/annurev.earth.28.1.211

Zhang, M., Guo, Z., Xu, S., Barry, P. H., Sano, Y., Zhang, L., et al. (2021). Linking deeply-sourced volatile emissions to plateau growth dynamics in southeastern Tibetan Plateau. *Nat. Commun.* 12, 4157. doi:10.1038/s41467-021-24415-y

Zhang, P. Z., Shen, Z., Wang, M., Gan, W., Bürgmann, R., Molnar, P., et al. (2004). Continuous deformation of the Tibetan Plateau from global positioning system data. *Geol.* 32, 809–812. doi:10.1130/g20554.1

Zong, G., Chen, W., Huang, X., and Xu, Q. (1996). *Cenozoic mammals and environment of hengduan mountains region*. Beijing: Ocean Press.